Automatic Human Knee Cartilage Segmentation From 3-D Magnetic Resonance Images

Pierre Dodin, Jean-Pierre Pelletier, Johanne Martel-Pelletier*, and François Abram

***Abstract*—This study aimed at developing a new automatic segmentation algorithm for human knee cartilage volume quantification from MRI. Imaging was performed using a 3T scanner and a knee coil, and the exam consisted of a double echo steady state (DESS) sequence, which contrasts cartilage and soft tissues including the synovial fluid. The algorithm was developed on MRI 3-D images in which the bone–cartilage interface for the femur and tibia was segmented by an independent segmentation process, giving a parametric surface of the interface. First, the MR images are resampled in the neighborhood of the bone surface. Second, by using texture-analysis techniques optimized by filtering, the cartilage is discriminated as a bright and homogeneous tissue. This process of excluding soft tissues enables the detection of the external boundary of the cartilage. Third, a technology based on a Bayesian decision criterion enables the automatic separation of the cartilage and synovial fluid. Finally, the cartilage volume and changes in volume for an individual between visits was assessed using the developed technology. Validation included first, for nine knee osteoarthritis patients, a comparison of the cartilage volume and changes over time between the developed automatic system and a validated semi-automatic cartilage volume system, and second, for five knee osteoarthritis patients, a test–retest procedure. Data revealed excellent Pearson correlations and Dice similarity coefficients (DSC) for the global knee ($r = 0.96$, $p < 0.0001$, and median DSC $= 0.84$), for the femur ($r = 0.95$, $p < 0.0001$, and median DSC $= 0.85$), and the tibia ($r = 0.83$, $p < 0.0001$, and median DSC $= 0.84$). Very good similarity between the automatic and semi-automatic methods in regard to cartilage loss was also found for the global knee ($r = 0.76$ and $p = 0.016$) as well as for the femur ($r = 0.79$ and $p = 0.011$). The test–retest revealed an excellent measurement error of $-0.3 \pm 1.6\%$ for the global knee and $0.14 \pm 1.7\%$ for the femur. In conclusion, the newly developed fully automatic method described herein provides accurate and precise quantification of knee cartilage volume and will be a valuable tool for clinical follow-up studies.**

***Index Terms*—Cartilage volume, image resampling, magnetic resonance imaging (MRI), texture analysis, surface parameterization, three-dimensional segmentation.**

I. Introduction

OSTEOARTHRITIS is a common cause of disability in people aged over 60 years [1]. Knee osteoarthritis is a prevalent disease characterized by cartilage degradation. Although this disease is often considered benign, severe degenerative changes may cause serious disability. Several pharmacologic drugs aimed at retarding or inhibiting the progression of joint tissue structural changes are under development to treat osteoarthritis. In this context, quantitative cartilage damage assessment is of significant importance for monitoring the progression of this disease and for evaluating therapeutic response.

The current gold standard for measuring cartilage thickness remains the radiographic method [2], [3], which allows the measurement of the joint space width (JSW). However, this technique has several significant limitations in that it allows the assessment of cartilage loss only on the focal weight bearing area of the joint and demonstrates weak sensitivity to change. Another technique, MRI, allows precise visualization of joint structures, including the cartilage and its pathological changes. In recent years, there have been a series of advances in the use of optimized MRI acquisition sequences to assess cartilage volume and thickness in patients with knee osteoarthritis [4]. Recently, a semi-automatic system was developed and used for the quantitative assessment of knee cartilage volume in observational, longitudinal, and clinical studies [5]–[16]. The accuracy and reliability of such a 3-D computer method was validated in a realistic measurement context [17]. However, a fully automatic system using MRI that prevents the intra- and interreader variations will enable more stable measurements.

Folkesson *et al*. [18] and Grau *et al*. [19] proposed methods to automatically segment the knee cartilage as a single object using a two step multiclass classification scheme and a controlled watershed approach, respectively. However, such procedures are problematic if one wants to study the cartilage changes over time. These methods do not employ a registration reference that is stable over time, e.g., a bone surface, limiting evaluation to cartilage volume for each single visit, thus precluding evaluation of cartilage volume change over time. Moreover, these methods do not address the separation of the global cartilage into individual bone cartilage, i.e., femoral, tibial, and patellar cartilage. Recently, Fripp *et al*. [20] also described an automatic cartilage segmentation system based on the deformation of a statistic shape using the active shape modeling (ASM) method with *a priori* knowledge of the articular domain. This model based segmentation was validated only on healthy volunteers, and as pointed out by the authors, "diseased knees are more difficult to segment as osteophytes, lesions, and intensity inhomogeneities and cracks are often found." Recently, a non-model-based method was proposed by Li *et al*. [21]. They introduced a semi-automatic cartilage segmentation procedure in which the bone was first segmented from a set of

Manuscript received March 30, 2010; revised May 31, 2010; accepted June 29, 2010. Date of publication July 15, 2010; date of current version October 15, 2010. *Asterisk indicates corresponding author.*

P. Dodin and F. Abram are with ArthroVision Inc., Montreal, QC H2K 1B6, Canada (e-mail: pdodin@arthrovision.biz; fabram@arthrovision.biz).

J.-P Pelletier is with the Osteoarthritis Research Unit, University of Montreal Hospital Research Centre, Notre Dame Hospital, Montreal, QC H2L 4M1, Canada (e-mail: dr@jppelletier.ca).

*J. Martel-Pelletier is with the Osteoarthritis Research Unit, University of Montreal Hospital Research Centre (CRCHUM), Notre Dame Hospital, Montreal, QC H2L 4M1, Canada (e-mail: jm@martelpelletier.ca).

Digital Object Identifier 10.1109/TBME.2010.2058112

seed spheres, then the cartilage using a graph-based method. This method is, however, mainly validated for thickness measurements in closed object segmentation, for example, ankle cartilage, as reported in their study. In addition, the aforementioned methods [18]–[21] did not include the final separation of the cartilage from synovial fluid, which impairs the accurate delineation of cartilage. Finally, there was no comparison of the cartilage evolution over time with another validated segmentation method, nor test–retest precision evaluation. This work thus aims at developing a new technological fully automatic segmentation algorithm for human osteoarthritic knee cartilage volume quantification from MR images, taking into account the aforementioned problems.

II. Methods

For this study, the bone–cartilage interface for the femur, tibia, and patella is obtained by an independent segmentation process. Such bone segmentation of the 3-D MR images of the knee was previously described using automatic [22], [23] and semi-automatic [24] procedures; however, in this study, we used a recently developed automatic bone segmentation system, which consists of surface selection by a ray-casting method [25] and provides parameterized surfaces in cylindrical pattern. Briefly, the ray-casting algorithm searches surface samples by intersecting gradient images with rays launched from an initial position inside the region of interest. Using these surfaces as domains of potential presence of cartilage, named articular domains, the cartilage objects are located by selecting voxels with homogeneous texture characteristics near the surface. Indeed, if we define surface normal as the vectors perpendicular to surface's tangent vectors, the external boundary of the cartilage can be delineated by a texture analysis of each voxel along surface normal in a certain neighborhood. It is a matter of deciding whether voxels belong to the cartilage class or to another class. In contrast to another model approach [20], the absence of a prior model in our case allows the delineation of unpredictable cartilage morphology that typically occurs in osteoarthritis patients. To allow such processing based on texture analysis, the MR image is resampled in the neighborhood of the bone parametric surface for a consistent analysis of the structured tissue, i.e., the cartilage. The bone surface, called reference surface, will then provide a new 3-D coordinate system, in which the 2-D parametric coordinates of the surface correspond to the two first dimensions and the distance normal to the surface, "height," will be the third dimension. More precisely, this procedure computes an image of normal, with a discrete number of parallel layers, each layer being at a certain distance, height, from the reference surface. In this image, the cartilage consists of an object organized along parallel layers appropriate to a 2-D texture analysis in each of these layers. The spatial gray level dependence (SGLD) operators [26] are the most relevant operators for extracting the texture properties on each layer. The cartilage is thus represented as a bright and homogeneous tissue, contrasting other bright but inhomogeneous surrounding tissues and the homogeneous but dark bone.

At present, the MR sequences the most commonly used for cartilage volume assessment on 1.5T apparatus [27], [28] are gradient echo sequences, such as spoiled gradient recall (SPGR; GE, Milwaukee, WI), fast imaging at steady-state precession (FISP; Siemens, Erlangen Germany), or fast–low angle shot (FLASH). These sequences provide similar images, focusing on the contrast between cartilage and other articular tissues. In a large proportion of the images, a similar signal is provided for the cartilage and the synovial fluid and the procedure may select synovial fluid voxels in the cartilage object. The main challenge in cartilage segmentation is to separate cartilage from synovial fluid. Recently, the double echo steady state (DESS; Siemens) sequence was used on 3T apparatus for cartilage volume assessment, as it enhances the contrast between the cartilage and synovial fluid [29], [30]. For this study, the MR images were scanned on 3T apparatus using the DESS sequence. Our data showed that the cartilage can be automatically separated from the synovial fluid by using a Bayesian decision threshold in the intensity histogram of the mixed object. Based on the observation that cartilage belongs to the bright and homogeneous tissues and that synovial fluid belongs to the extra bright and homogeneous tissues, we were able to design a 1-D decision criterion to find a threshold.

We further describe a procedure that allows the automatic computation of the cartilage volume change for an individual with two or more MRI exams. In order to ensure a near perfect alignment of the maps in follow-up evaluation, we used a previously described registration procedure [31]. In addition, validation experiments were performed in which the cartilage volume of nine osteoarthritic knee patients at baseline and 12 months evaluated with the developed automatic system was contrasted with the results obtained using the validated semi-automatic method Cartiscope [17]. A test–retest analysis was also performed on five osteoarthritic knee patients.

Because the cartilage is a structured tissue, which covers surfaces of various geometries, i.e., femur, tibia, and patella, we estimated that its detection would be more accurate in images resampled along the supporting surface using texture analysis. Thus, Section III describes the geometric design of the images of normals resampled in the proximity of the parameterized bone surface, as well as the texture analysis. Section IV details the interpretation of the texture analysis in order to select the cartilage voxels. Section V describes the separation of cartilage and synovial fluid in the images using the DESS sequence, which enhances the cartilage to fluid contrast. Section VI explains a structural-filtering process, which enhances the filtering of misclassified voxels. Section VII explains the method for computing cartilage volume changes over time based on the analysis of two images of the same patient taken 12 months apart. Section VIII describes the validation experiments and the correlations obtained for the whole knee cartilage as well as for knee subregions, and Section IX concludes the paper.

III. Images of Normals

Let I be an MR image of the knee, where the cartilage must be segmented. Image I is a 3-D image, i.e., it is a discrete function of the Euclidian 3-D space, whose values are intensities such

that

$$\mathrm{I}(x,y,z) = l \quad (x,y,z) \in \mathsf{Z}^3. \tag{1}$$

Given a known and segmented bone surface ϕ, either femur and/or tibia in the same image I, the surface is described by two parameters (u, v) as follows:

$$(x,y,z) = \phi(u,v) \quad (x,y,z) \in \mathsf{R}^3. \tag{2}$$

The bone surface ϕ, used as a reference surface, allows us to define a volume of interest that contains the entirety of the cartilage. Indeed, a set of layers parallel to ϕ at a certain distance h of ϕ along the surface normals can be defined. Moreover, using the intrinsic parametric coordinate system of ϕ, the cartilage search will be performed in a parallelepiped domain of interest consisting of parallel layers. This domain can inherit the intensity properties of the original image I, thus creating a new resampled 3-D image. But, before proceeding, we will explain how the notion of voxel helps to transport I in R^3 preserving the same level of continuity of ϕ in the image I.

A. Definition of Voxel, Continuity of Image Signal

By nature, the information inside the 3-D MR image is digital, thus the indices (x, y, z) are integers. Hence, a set C obtained with the implicit equation using an intensity level l

$$V = \{(x,y,z)/\mathrm{I}(x,y,z) = l\} \tag{3}$$

is of course discrete. This is not compatible with the R^3 Euclidean geometry used in Section II. The compatibility is obtained using voxels. We will name voxels a collection of unit cubes in R^3, parallel to the coordinate axes and whose centers are in Z^3. Hence, V can be embedded as $\tilde{V}$, a continuous subset of R^3, whose centers are defined by C; for simplification reasons, we will identify $\tilde{V}$ and V.

B. Image of Normals J Obtained by Resampling of Image I

A resampling of the image I is performed along the reference surface, since we need to extract the information of intensity and contrast of this region of interest. Being a parametric 3-D surface, the reference surface is described by two parameters (u, v) as formulated by (2). A third dimension is necessary to define a volume that will be immersed in the original image I. To this end, the distance to the surface, *h*, height along the normal vectors to the surface ϕ, of value zero on the surface itself, was chosen. The normal vector to the surface can easily be defined by a cross product ($\wedge$) of the tangent vectors along each implicit parameter, i.e., $\overrightarrow{\partial\phi}/\partial u$ and $\overrightarrow{\partial\phi}/\partial v$. Both tangent vectors along implicit parameters as well as the normal to the surface are illustrated in Fig. 1. Thus, the extended map is defined as follows:

$$\Phi(u,v,h) = \phi(u,v) + h\frac{\overrightarrow{\partial\phi}}{\partial u} \wedge \frac{\overrightarrow{\partial\phi}}{\partial v.} \tag{4}$$

The extended map $\Phi(u, v, h)$ links voxels expressed in the (u, v, h) parametric system and the voxels in the (x, y, z) 3-D initial coordinate system. Now, using the function Φ, a new

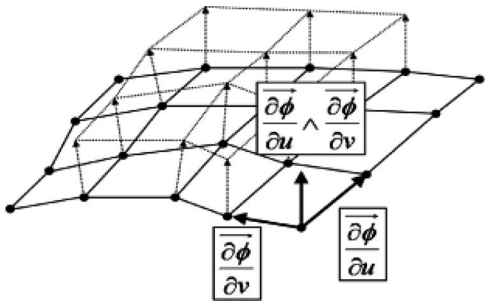

Fig. 1. Parameterized surface, the two tangent vectors $\overrightarrow{\partial\phi}/\partial u$ and $\overrightarrow{\partial\phi}/\partial v$ and the normal vector $\overrightarrow{\partial\phi}/\partial u \wedge \overrightarrow{\partial\phi}/\partial v$.

Fig. 2. Original signal resampled along the normals of a femur bone surface. Illustration of one slice of $J(u, v, h)$ for a given u.

volume $J(u, v, h)$ can be computed as follows:

$$J(u,v,h) = \mathrm{I} \circ \Phi(u,v,h). \tag{5}$$

Thus, the original image $\mathrm{I}(x, y, z)$ is locally transformed in a resampled image $J(u, v, h)$ using the predefined parametric coordinate system. Fig. 2 shows a slice of the 3-D image J for a given u.

C. K, the Contrast Matrix of J

In order to obtain the texture characteristics for each voxel, the "layer-by-layer" 2-D analysis of the volume of interest can be performed, analyzing each layer separately. This allows the dimension of the analysis to be reduced. Using the SGLD technique detailed in Appendix I, a global contrast value can be obtained for a layer of the image of normals J at a given height h. However, the analysis can be improved by performing a local assessment of the contrast by using neighborhoods of (u, v), which when applied to each voxel at height h, allows a matrix of contrast of the same size as the layer. The calculus leads to a contrast matrix of the entire image of normals, named $K(u, v, h)$ defined in (29), Appendix II.

Example: From image of normals J (see Fig. 2) of a femur bone surface, the analysis of intensity provides the bright-tissue mask, as illustrated in Fig. 3. The texture analysis of J restricted to the masked volume produces the matrix of contrast K shown in Fig. 4.

IV. Cartilage Segmentation Based on Bright and Homogeneous Tissues

To select cartilage voxels in an MR image, we must be able to separate them from voxels of other tissues based on the signal characteristics of the volume of interest. Using the intensity

Fig. 3. Selection of the bright tissues from the original image, shown as white in the figure, corresponds to the high-intensity voxels. Note that the black pixels of this image are excluded from further contrast analysis.

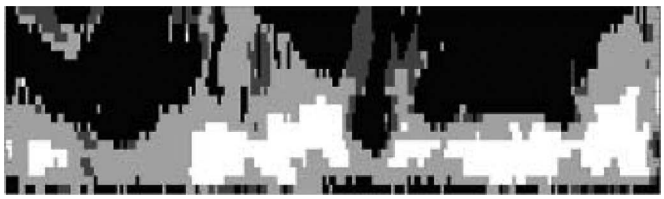

Fig. 4. Contrast information is computed on the bright tissues selected previously (see Fig. 3). Slice of contrast matrix $K(u, v, h)$ for a given u. In this image, white reveals bright tissues with high homogeneity, light gray, bright tissues with regular homogeneity, and dark gray inhomogeneous tissues.

does not provide enough information to accurately distinguish cartilage voxels. However, the contrast provides pertinent information for the voxel selection. In this section, we explain how bright and homogeneous tissues allow the discrimination of the cartilage from other tissues. This is why we will consider this class of tissue to provide the first estimate for the segmentation of the cartilage. We will see later that other tissues are included in this class, thus requiring a second discrimination analysis.

A. Observations on Bright and Homogeneous Tissues

We were first interested in the bright and homogeneous tissues when studying direct thresholding of the MR images. Intensity analysis of a single slice of a sagittal knee MR image scanned with fat suppression always gives two contrasted classes of gray levels: bright and dark tissue intensities. Bright intensities correspond to cartilage and surrounding soft tissues, while dark intensities correspond to bone and other tissues of noninterest. Threshold modification impacts the image structure in such a way that soft tissues disappear discontinuously, while cartilage disappears by wide zones. A closer analysis reveals that, in the darker components of the soft tissues, there are probably drier parts that make them inhomogeneous. By giving a variational meaning to this inhomogeneity, one can predict that a small spatial displacement will result in a change in the gray level. This change could be detected with texture-analysis methods, i.e., spatial gradient of the intensity analysis. This measurement demonstrated higher gradient values for the soft tissues than for the cartilage, which led us to investigate the bone–cartilage interface contrast using the texture analysis.

The 2-D analysis of the texture in the layers of the image of normals is logical as the texture will be evaluated in parallel to the interface that we want to localize, making its detection more precise. Thus, for each voxel of J, we attribute a variational criterion, i.e., the contrast value computed on a neighborhood in each layer. It will allow the limit of the cartilage along the normal to be found. Moreover, the volume of interest limits the false negative as it focuses on a volume near the articular domain.

B. Bright and Homogeneous Tissue Evaluation

This section describes the selection of the cartilage volume in the image of normals J in which we want to find a threshold S_l that separates dark from bright tissues in the intensity domain. The intensity level histogram H_l of the images allows the statistical characteristics of two Gaussian contributions in a complex distribution to be computed using the Otsu algorithm [32]. Thus, applied to the intensity level histogram of J defined in (5), the Otsu algorithm decomposes it as a mix of two principal components in the intensity domain: Gaussian distributions $N(\mu_1^l, \sigma_1^l)$ dark tissues, and $N(\mu_2^l, \sigma_2^l)$ bright tissues, as follows (p is a mixing parameter):

$$H_l \cong pN(\mu_1^l, \sigma_1^l) + (1-p)N(\mu_2^l, \sigma_2^l). \tag{6}$$

The separation threshold S_l is chosen as the most probable threshold between the two distributions. When applying this threshold to the image, we obtain the object of bright tissues

$$\mathrm{BO} = \{(u, v, h)/J(u, v, h) \geq S_l\}. \tag{7}$$

In complement to S_l, μ_2^l is used as a lower threshold for very bright tissues.

With the same method, on the histogram H_t of texture image K introduced in Section III-C and defined by (29) in Appendix II, we can apply the Otsu algorithm to compute the separation between homogeneous and inhomogeneous tissues in the texture domain. Thus, the Otsu algorithm decomposes the histogram H_t as a mix of two Gaussian distributions $N(\mu_1^t, \sigma_1^t)$ homogeneous tissues, and $N(\mu_2^t, \sigma_2^t)$ inhomogeneous tissues, as follows (q is a mixing parameter):

$$H_t \cong qN(\mu_1^t, \sigma_1^t) + (1-q)N(\mu_2^t, \sigma_2^t). \tag{8}$$

The separation threshold S_t is chosen as the most probable threshold between the two distributions. When applying this threshold to the image, we obtain the object of homogeneous tissues:

$$\mathrm{HO} = \{(u, v, h)/K(u, v, h) \leq S_t\}. \tag{9}$$

In complement to S_t, μ_1^t is used as a higher threshold for very homogeneous tissues.

The 3-D object corresponding to bright and homogeneous tissues BHO, can be defined as the intersection of the two subsets BO and HO

$$\mathrm{BHO} = \mathrm{BO} \cap \mathrm{HO}. \tag{10}$$

This statistical interpretation reveals the classes of tissues shown in Table I that were verified in the images.

TABLE I
CLASSES OF TISSUES

	Very homogeneous	Homogeneous	Inhomogeneous
Very Bright	Water	Water Cartilage	
Bright	Water Cartilage	Cartilage	Soft tissues
Dark		Dark cartilage Cartilage lesion	Cartilage lesion

C. Definition of Cartilage Volume for Femur and Tibia

The selection criteria being defined for the cartilage, i.e., bright and homogeneous tissues, we then process the image of normals for both bones, i.e., femur and tibia.

Knowing the parameterization of the surfaces of both femur and tibia in the cylindrical coordinate system, Φ_F and Φ_T respectively, corresponding images of normals J_F and J_T are computed by resampling the original image $\mathrm{I}(x, y, z)$ along the samples (u, v, h) and (u', v', h'), where u (u') represents the position on the cylindrical axis, v (v') represents the angle, and h (h') represents the height along the normal vectors to the surface ϕ

$$\begin{aligned} J_F(u, v, h) &\equiv \mathrm{I} \circ (\Phi_F(u, v, h)) \\ J_T(u', v', h') &\equiv \mathrm{I} \circ (\Phi_T(u', v', h')). \end{aligned} \tag{11}$$

The maximum height is chosen in such a way that the entire relevant information with regard to the cartilage is considered. It is important to set h to the distance between the two bone surfaces to allow further processing. For example, with a height of 40 voxels and a resolution of 0.3 mm, a h of 12 mm is then a pertinent choice.

Once the maximum height is defined, matrices of normals J_F and J_T are computed followed by the evaluation of texture matrices $K_F(u, v, h)$ and $K_T(u', v', h')$ according to (29) in Appendix II. Let us call F and T be the cartilage object of the femur and of the tibia. These sets are defined by the following relations, with $\lambda = (u, v, h)$ and $\mu = (u', v', h')$ to reduce notations

$$\begin{aligned} F &= \{\lambda / J_F(\lambda) \geq S_l\} \cap \{\lambda / K_F(\lambda) \leq S_t\} \\ T &= \{\mu / J_T(\mu) \geq S_l\} \cap \{\mu / K_T(\mu) \leq S_t\}. \end{aligned} \tag{12}$$

In this step, the objects F and T do not separate the cartilage from the femur and the tibia. The processing done so far consisted of a selection around the reference surfaces of each bone Φ_F and Φ_T. The segmentations of the cartilage from the femur F and from the tibia T share some information in that there is a part of F in T and a part of T in F. In order to separate the cartilage of the femur from that of the tibia, the transformations between J_F and J_T must be evaluated. Thus, the selected voxels can be transported to the alternate analysis volume, i.e., femur parametric coordinate system to tibia parametric coordinate system and *vice versa*. Hence, the common volume is first located. Then, within this volume, where both femur and tibia information is overlapped, it is decided that half the thickness belongs to the femur and half to the tibia. Since the patella is given by the bone segmentation, the same separation process is done to separate the femoral cartilage from the patellar cartilage, using the patella surface.

In this step, the result of segmentation appears to be final. However, another step is required to extract the synovial fluid at the cartilage–synovial fluid interface.

V. EXCLUSION OF SYNOVIAL FLUID

In contrast to the MR sequences used in a 1.5T apparatus, such as the SPGR, which do not contrast the synovial fluid, the DESS sequence allows a good contrast between the bone and the cartilage, and enhances the contrast between the cartilage and the synovial fluid [28], [29], providing sufficient difference between these tissues to allow automatic separation of the two classes.

A. DESS Sequence Allows Synovial Fluid/Cartilage Discrimination

In DESS MR images, the intensity of the synovial fluid appears to be slightly greater than the cartilage, thus there exists a detection threshold. This threshold does not appear clearly in the histogram of intensity of the image J, but several tests revealed that the contrast image K is a valuable image to find the information that the synovial fluid is an even more homogeneous tissue than the cartilage.

Indeed, in DESS MR images, the synovial fluid objects are uniformly very bright within a range of voxels. Thus, the very homogeneous voxels consist mostly of synovial fluid; the cartilage, however, appears as the minority. This allows the identification of two classes defined by $C_{\mathrm{wat}} = \{\lambda / K(\lambda) \leq \mu_1^t\}$ is class of very homogeneous tissues and $C_{\mathrm{cart}} = \{\lambda / K(\lambda) > \mu_1^t\}$ is class of not very homogeneous tissues (λ is used in place of (u, v, h) to simplify the notations), which allows two densities of probability, given by image histogram defined by

$$\begin{aligned} P_{\mathrm{wat}}(l) &= P(J(\lambda) = l | \lambda \in C_{\mathrm{wat}}) \\ P_{\mathrm{cart}}(l) &= P(J(\lambda) = l | \lambda \in C_{\mathrm{cart}}) \end{aligned}. \tag{13}$$

These densities are a function of the intensity l and named $P_{\mathrm{wat}}(l)$ and $P_{\mathrm{cart}}(l)$. We are looking for a decision test enabling the intensity threshold to be defined, which will discriminate the synovial fluid voxels in order to subtract them from the F and T sets.

B. Synovial Fluid Discrimination Using Statistical Test

Using a Bayesian test, we are able to obtain the intensity l that provides the optimal statistical threshold between the two classes, i.e., cartilage and synovial fluid.

The Bayesian test states that λ belongs to class C_{wat}, for a given l if

$$P(\lambda \in C_{\mathrm{wat}} | J(\lambda) = l) \geq P(\lambda \in C_{\mathrm{cart}} | J(\lambda) = l). \tag{14}$$

We note $c_{\mathrm{cart}} = P(\lambda \in C_{\mathrm{cart}})$ and $c_{\mathrm{wat}} = P(\lambda \in C_{\mathrm{wat}})$ are the prior probability. Using Bayes theorem, the Bayesian test

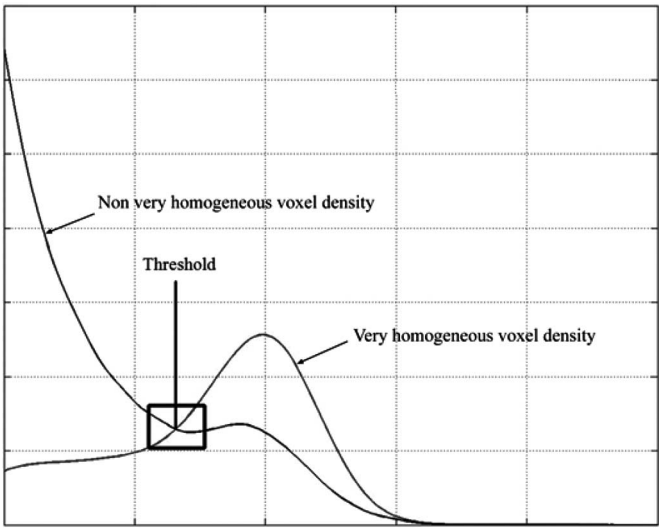

Fig. 5. Densities $P_{\mathrm{cart}}(l)c_{\mathrm{cart}}$ and $P_{\mathrm{wat}}(l)c_{\mathrm{wat}}$ function of intensity l, and the computed threshold.

can be rewritten as a hypothesis test

$$\frac{P_{\mathrm{cart}}(l)}{P_{\mathrm{wat}}(l)} \geq \frac{c_{\mathrm{wat}}}{c_{\mathrm{cart}}}. \tag{15}$$

To evaluate the second member of (15), we divide the cardinal of class c_{wat} by the cardinal of class c_{cart}. Thus described, this test is operational and allows the optimal threshold l that separates the cartilage from the synovial fluid to be found. Fig. 5 shows that the test formalized by (15) consists of finding the intersection between the distributions of the two curves $P_{\mathrm{cart}}(l)c_{\mathrm{cart}}$ and $P_{\mathrm{wat}}(l)c_{\mathrm{wat}}$. The initial histogram of the image shows the existence of voxels with very high intensity; these voxels correspond to the fluid. The two curves $P_{\mathrm{cart}}(l)c_{\mathrm{cart}}$ and $P_{\mathrm{wat}}(l)c_{\mathrm{wat}}$ are the decomposition of the histogram, $P_{\mathrm{wat}}(l)c_{\mathrm{wat}}$ being the part corresponding to the fluid.

The segmentation process is now completed, enabling the cartilage volume evaluation and its changes over time, excluding the volume of synovial fluid.

VI. Final Filtering

Variability may occur due to incorrect classification, i.e., false alarms or missed detections, which occur locally as a consequence of weak contrast delineation between tissues and are mainly due to a low signal-to-noise ratio. In order to obtain the best results, a filtering procedure must be applied to the computed cartilage object.

We have observed that edges searched inside normal image J give valuable information about the external cartilage interface. Starting below the surface level toward the exterior, the first edge information is the bone to cartilage interface, and the second is the cartilage to soft tissues interface.

Unfortunately, the sparse structure of the edge prevents its use for initial cartilage search. However, if we combine this information with the objects obtained by texture analysis, we acquire excellent results. We start from $\mathbf{F}(u, v, h)$, the femoral cartilage binary matrix, such that $F = \{(u, v, h)/\mathbf{F}(u, v, h) = 1\}$.

Fig. 6. Slice of the image of normals.

Fig. 7. Initial solution is highlighted.

Fig. 8. Binary-edge information is highlighted.

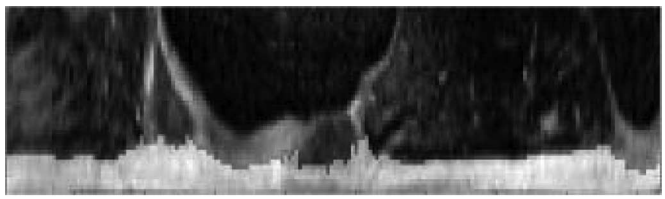

Fig. 9. Correction result using edge information.

A. Filtering Procedure

The procedure, explained step-by-step from Figs. 6–10, is sequenced as follows.

1) Femoral cartilage volume F search, obtained by texture analysis. The result is shown in Fig. 7 and is obtained from the initial slice information of J illustrated in Fig. 6.
2) Binary edge image ΔJ computation shown in Fig. 8 and defined in Appendix III.
3) External interface correction, along each normal (u, v) of J. If two edges are found inside F, these edges become the new boundaries of F, as illustrated in Fig. 9.
4) Smoothing, for each height h, the surface of all 2-D restrictions of F to height h are filtered against small parts based on the area of each individual contribution. Final result is shown in Fig. 10.

It should be noted that in Fig. 9, there is a possibility that the correction procedure failed locally; the absence of measurement did not allow separation of a subpart of a meniscus. It is the

Fig. 10. Correction result and component surface filtering.

counterpart of the boundary-detection approach. In the filtering procedure, this is further overcome by the surface smoothing.

However, as shown in Fig. 11, this approach succeeded in finding complex cartilage morphology, by taking into account only measurement and not prior cartilage morphology.

B. Final Segmentation Examples

Examples of segmentation for two patients as calculated by the presented technology are shown in Fig. 12.

In brief, the resampling process transforms the original image into another coordinate system defined by the bone surface. This step enables the "layer-by-layer" analysis and makes continuous assessment of cartilage volume change simpler and more convenient.

VII. Cartilage-Change Detection

One of the main purposes of quantifying the volume of cartilage and using noninvasive means such as MR images is to study its temporal evolution for observational and longitudinal studies. To allow comparison of cartilage volume for an individual from MR images obtained at different times, analysis should be performed in the same parametric space.

A. Registration Between Bone Surfaces

The images of an individual at two dates t_1 and t_2 should be computed using a registration function to obtain a spatial correspondence between bone surfaces to compensate for the different positioning of the individual during each exam. We suppose bone surfaces ϕ_{t1} and ϕ_{t2} of the femur and tibia have been extracted from the two images $\mathrm{I}(t_1)$ and $\mathrm{I}(t_2)$. There exists a registration function R allowing surface superposition. Registration using the iterative closest point method (ICP) [33] was performed in the image coordinate space. Using (4), we compute extended maps $\Phi_{t_1}(u,v,h)$ and $R\Phi_{t_1}(u,v,h)$ from which images of normals can be constructed in the same parametric space

$$\begin{aligned} J_1(u,v,h) &= \mathrm{I}(t_1) \circ \Phi_{t1}(u,v,h) \\ J_2(u,v,h) &= \mathrm{I}(t_2) \circ R\Phi_{t1}(u,v,h). \end{aligned} \tag{16}$$

This procedure allows the analysis of cartilage evolution in the same parametric space, thus limiting variability due to misalignment in the follow-up evaluation.

B. Cartilage Volume Change Computation

When the filtering process is completed, we obtain two segmentation results for t_1 $[F_1, T_1]$, and two for t_2 $[F_2, T_2]$, respectively, for the femur and tibia cartilage objects for visit t_1 and t_2. Using registration functions R_{femur} and R_{tibia}, we can compare F_1 and F_2 or T_1 and T_2, as they are in the same parametric space. Following is the computation of cartilage volume change in which we describe the volume computation method.

The volume of the cartilage object in voxels is expressed as follows for the femur as an example:

$$\mathrm{vol}_{\mathrm{voxel}}(F_k) = \sum_{u,v,h} \mathbf{F}_k(u,v,h). \tag{17}$$

In order to obtain a volume in cubic millimeter, the cartilage object, described by its extended map, must be transported from the pixel coordinates into the millimeter coordinates using a linear transformation T_{mm}

$$\Phi^{\mathrm{mm}}(u,v,h) = T_{\mathrm{mm}}\,\Phi\,(u,v,h). \tag{18}$$

The volume computed in a neighborhood of $\Phi^{\mathrm{mm}}(u,v,h)$ was evaluated as the volume of polyhedron $\mathbf{P}(u,v,h)$, whose vertices belongs to $\{\Phi^{\mathrm{mm}}(u \pm 1/2, v \pm 1/2, h \pm 1/2)\}$, as explained in Appendix IV and obtained in cubic millimeter as follows:

$$\mathrm{vol}(F_k) = \sum_{u,v,h} \mathrm{vol}(\mathbf{P}(u,v,h))\mathbf{F}_k(u,v,h). \tag{19}$$

Once F_1 and F_2 are restricted by an intersection mask to the same bidimensional surface domain (u,v), the cartilage loss in percentage is defined by

$$\mathrm{Loss} = 100 \times \frac{\mathrm{vol}(F_2) - \mathrm{vol}(F_1)}{\mathrm{vol}(F_1)}. \tag{20}$$

Note that the eventual cartilage "holes," areas without cartilage surrounded by cartilage, are included in each domain as areas with cartilage of thickness null. The volumes and the changes over time were analyzed for the global knee, the femur and the tibia. To visually illustrate the pertinence and accuracy of the described procedure, the cartilage segmentation and cartilage loss detection are represented in Fig. 13. Of note, the automatic segmentation time for two visits of the same patient is approximately 1.5 h, including approximately 50 min for both bone segmentations, i.e., femur and tibia, less than 2 min for registration, and 40 min for both cartilage segmentations.

VIII. Validation

A cohort of 14 osteoarthritic patients aged 52 to 72 (62 ± 6.8 years) was used for the validation experiments. All patients were diagnosed by a certified rheumatologist as having osteoarthritis according to the American College of Rheumatology criteria [34]. This study was approved by the ethical research committee Regroupement Neuroimagerie/Quebec (CMER/RNQ), in Montreal, QC, Canada. A consent form was signed by each individual. The MRI exam, performed on a 3T MRI apparatus, included a sagittal 3-D DESS-water excitation (WE) sequence, ST $= 0.7$ mm, TR $= 16.32$ ms, TE $= 4.71$ ms, NEX $= 1$,

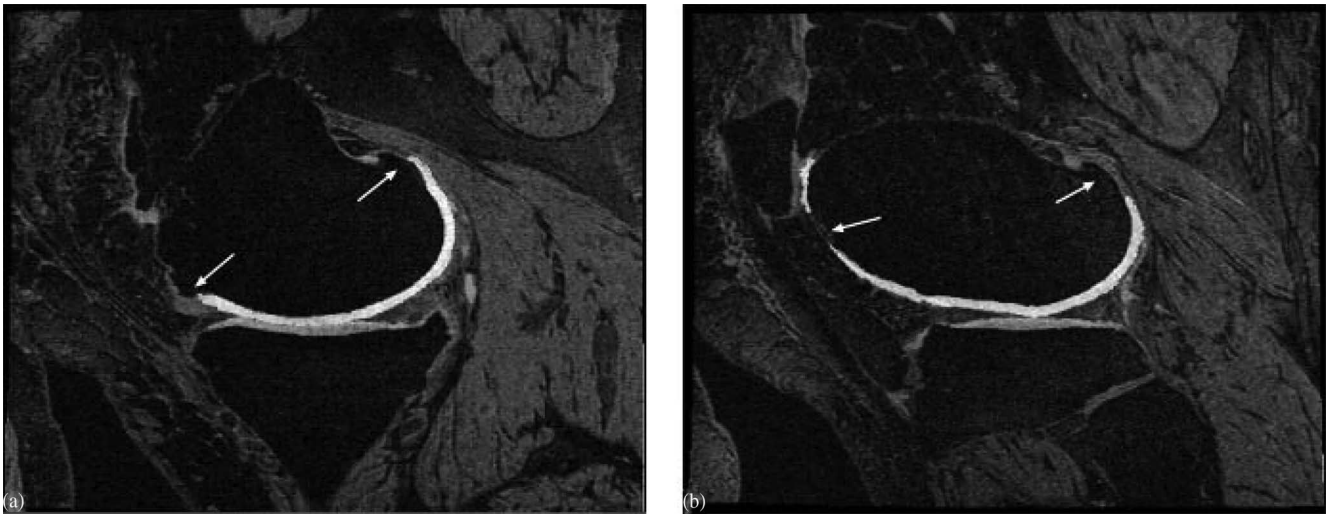

Fig. 11. Complex cartilage delineation: discontinuity provoked by (a) osteophytes and (b) denuded surface and osteophytes are indicated by arrows in the respective panels.

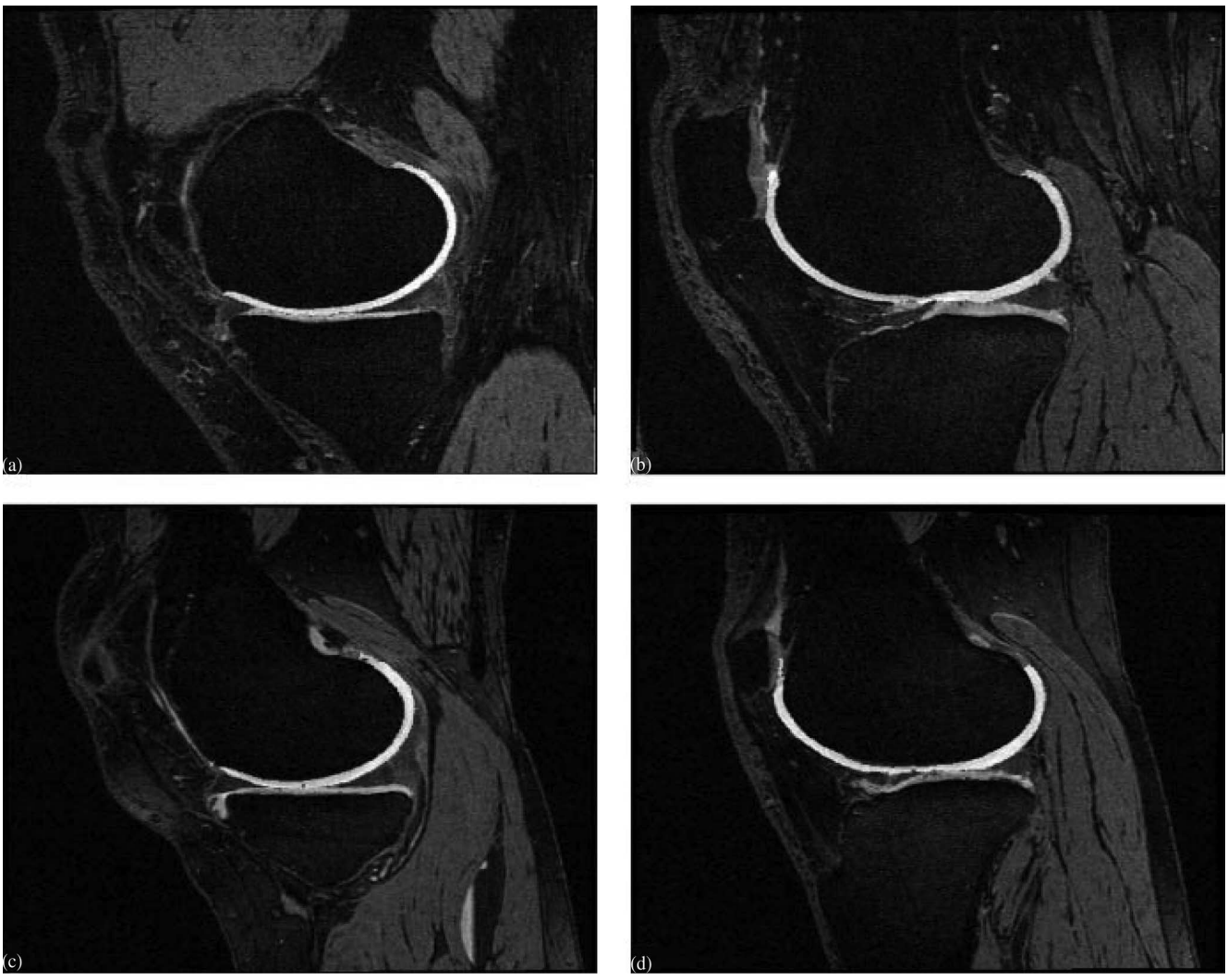

Fig. 12. Cartilage segmented with the newly developed automatic algorithm is shown in light gray for the femur and in darker gray for the tibia. Images represent patient 1 (a, b) and patient 2 (c, d), medial (a, c), and lateral (b, d) compartments.

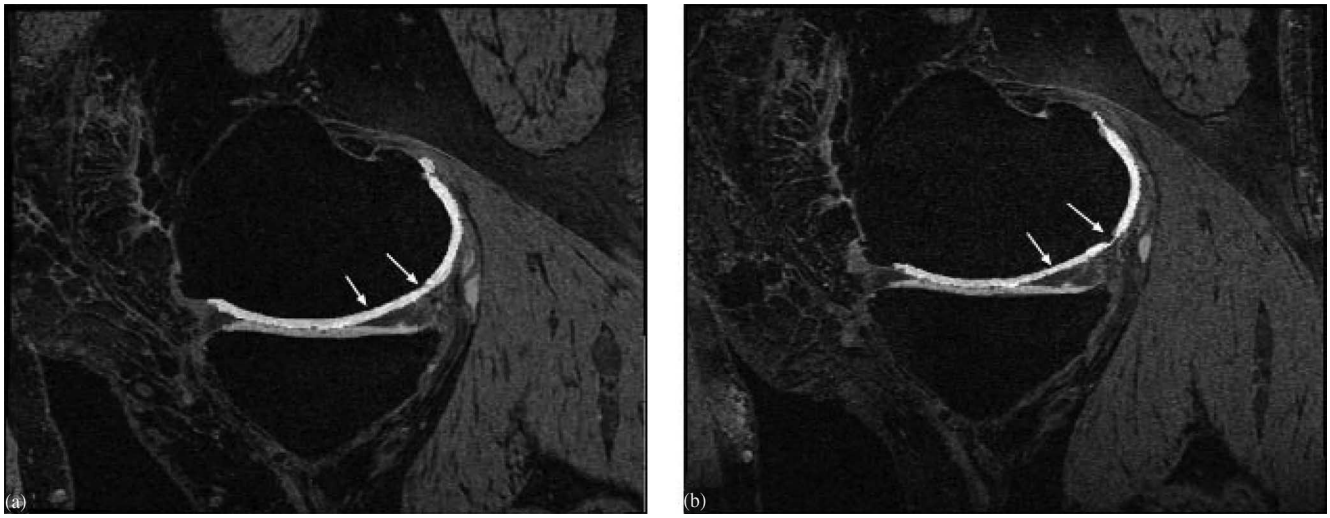

Fig. 13. MR images of an osteoarthritic individual showing medial femur loss of cartilage thickness near the posterior meniscus region between (a) the baseline and (b) 12-month follow-up. Arrows indicate the cartilage loss.

FoV = 140 mm, %phaseFoV = 100%, matrix = 384 px, phase resolution = 80%, FA = 25 deg, FS = WE, and phase partial Fourier = 7/8. This sequence is known to be optimized for cartilage reading [29].

The validation consisted of two parts. For the first part, a comparison of the cartilage volume, as well as volume changes over time, was performed between the validated semi-automatic method (Cartiscope) as previously described [31] and the newly developed fully automatic segmentation using scans from nine patients. For the second part, the measurement error of the newly developed segmentation was evaluated with a test–retest analysis using scans from five patients.

A. Comparison Between Automatic and Semi-Automatic Segmentations

Scans from nine osteoarthritic patients for which two MRIs of the same knee were done at a 12 month interval were used for cartilage volume evaluation with both the validated semi-automatic method (Cartiscope) and the newly developed automatic method. Table II shows the cartilage volume obtained for each visit for each patient. Patients are referred to as P1 to P9 and the MRI exams as baseline and visit, providing a total of 18 images, nine baseline, and nine follow-up visits. The correlation between the automatic and the semi-automatic segmentations was excellent with Pearson correlations of $r = 0.96$, $p < 0.0001$; $r = 0.95$, $p < 0.0001$; and $r = 0.83$, $p < 0.0001$ for the global knee, femur, and tibia, respectively.

For the nine patients, using (20), a vector of nine change-in-time values is obtained for each method. Data revealed an excellent correlation between the automatic and the semi-automatic method, for the global knee ($r = 0.76$ and $p = 0.016$) and for the femur ($r = 0.79$ and $p = 0.011$). No statistically significant correlation was found for the tibia. The latter could be explained as follows. First, the tibial plateau cartilage demonstrates a lower signal-to-noise ratio than the femoral condyle cartilage, i.e., the cartilage appears darker and is harder to distinguish from the other tissues, potentially resulting in incorrect classification of the pixels. Second, the articulation geometry is such that most of the tibia cartilage surface is in contact with the femur cartilage causing the higher measurement noise occurring in this area to weigh proportionally more for the tibial cartilage selection than for the femoral cartilage. Note that this noisy area has no impact at all on the global volume, which is the sum of both tibial and femoral cartilages. On the other hand, the Dice similarity coefficient (DSC) was computed as $\mathrm{DSC}(A, B) = 2 \times |A \cap B|/(|A| + |B|)$ as described in [18] for all regions. This coefficient measures spatial volume overlap between two segmentations. The DSC between automatic and semi-automatic segmentation showed values of 0.83 ± 0.04 (median 0.84) for the global, 0.84 ± 0.03 (median 0.85) for the femur, and 0.82 ± 0.07 (median 0.84) for the tibia. These results are similar to those of Fripp *et al*. [20] on a small number of healthy individuals: 0.85 ± 0.07 (median 0.87) for the femur and 0.83 ± 0.08 (median 0.85) for the tibia, as well as those of Folkesson *et al*. [18] obtained, on 86 non or mild osteoarthritis patients: 0.80 ± 0.03 for the global.

B. Test–Retest Experiment

Scans from five osteoarthritic patients for which two MRIs were done for both knees in the same exam with repositioning of the patient between the scans were used for cartilage segmentation with the newly developed automatic method. The knees are referred to as L1 to R5 for the left (L) and right (R) knees of patients 1 to 5. Patient 4 had three acquisitions of the right knee and none of the left; thus we considered two independent pairs, R4 for the comparison between test and the first retest, and R4B for the comparison between test and the second retest.

The measurement error evaluated according to the loss function (20) provides the average value and the standard deviation. Although the number of specimens was low, excellent values were obtained: $-0.30 \pm 1.6\%$ for the global knee and $0.14 \pm 1.7\%$ for the femur. For the tibial plateau, a test–retest

TABLE II
COMPARISON OF CARTILAGE VOLUME BETWEEN SEMI-AUTOMATIC AND AUTOMATIC METHODS FOR GLOBAL KNEE, FEMUR, AND TIBIA

GLOBAL	P1	P2	P3	P4	P5	P6	P7	P8	P9
BASELINE									
Semi-automatic (mm^3)	18351	12018	11108	19400	13283	21023	19032	18167	13141
Automatic (mm^3)	17814	12111	11239	18285	13447	19670	19637	15602	12120
DSC	0.88	0.79	0.85	0.82	0.81	0.87	0.87	0.75	0.86
VISIT (12 MONTHS)									
Semi-automatic (mm^3)	18643	10903	10852	18478	12997	19304	19662	18737	13539
Automatic (mm^3) (mm^3)	17470	11823	11141	17964	13207	18680	19435	15820	12350
DSC	0.88	0.80	0.83	0.81	0.88	0.85	0.85	0.74	0.84

FEMUR	P1	P2	P3	P4	P5	P6	P7	P8	P9
BASELINE									
Semi-automatic (mm^3)	12596	8887	7924	14397	10001	14907	13564	13484	10001
Automatic (mm^3)	12924	9385	8224	13174	9417	14800	13071	11776	9372
DSC	0.86	0.84	0.86	0.78	0.82	0.88	0.86	0.77	0.85
VISIT (12 MONTHS)									
Semi-automatic	12868	8201	7784	13385	9848	13655	13840	13892	10344
Automatic	12859	9177	8205	13076	9309	14207	12995	11888	9646
DSC	0.87	0.83	0.85	0.79	0.82	0.88	0.86	0.79	0.85

TIBIA	P1	P2	P3	P4	P5	P6	P7	P8	P9
BASELINE									
Semi-automatic (mm^3)	5754	3131	3184	5003	3282	6116	5468	4683	3140
Automatic (mm^3)	4890	2726	3016	5111	4029	4869	6566	3827	2748
DSC	0.89	0.70	0.84	0.88	0.80	0.84	0.88	0.71	0.87
VISIT (12 MONTHS)									
Semi-automatic (mm^3)	5774	2702	3068	5093	3150	5649	5823	4845	3195
Automatic (mm^3)	4611	2646	2936	4888	3898	4472	6440	3932	2704
DSC	0.88	0.75	0.86	0.88	0.80	0.82	0.85	0.64	0.82

TABLE III
TEST-RETEST CARTILAGE VOLUME (MM^3) FOR GLOBAL KNEE, FEMUR, AND TIBIA

GLOBAL	L1	R1	L2	R2	L3	R3	R4	R4B	L5	R5
TEST	9027	7810	7823	6317	8978	6709	9483	9483	7515	9701
RETEST	8885	7816	7589	6341	8804	6852	9414	9581	7464	9797

FEMUR	L1	R1	L2	R2	L3	R3	R4	R4B	L5	R5
TEST	6588	6129	7282	5435	6032	4181	7916	7916	5810	8008
RETEST	6594	6209	7044	5402	6051	4276	7898	8011	5724	8152

TIBIA	L1	R1	L2	R2	L3	R3	R4	R4B	L5	R5
TEST	2439	1681	540	882	2946	2528	1567	1567	1705	1694
RETEST	2291	1607	545	939	2753	2575	1516	1571	1740	1645

of $-1.12 \pm 3.8\%$ was found, which reflects the problems as described in Section VIII-A. Moreover, the minimum threshold for a detectable cartilage volume change according to the formula of Eng [35], in which the calculation was performed using the standard deviation of the global cartilage volume loss (1.6%) combined with a confidence probability of 95%, a statistical power of 85%, and 100 osteoarthritis patients (which is the average number of an osteoarthritis cohort in a clinical trial), is 0.96%.

IX. Conclusion

Here, we present an algorithm that automatically segments human knee cartilage from 3-D MR images, allowing continuous assessments of human osteoarthritic knee cartilage volume. Based on a presegmented bone surface, the method resamples the MR images within its neighborhood and uses texture analysis to detect the external boundary of the cartilage, followed by the automatic separation of the cartilage and the synovial fluid using a Bayesian decision criterion. Moreover, this system allows the quantification, not only of the global knee cartilage volume, but also of the femur and tibia independently.

In previously published works on automatic segmentation of articular cartilage [18]–[20], the methods did not allow a registration reference or separation of the knee cartilage into individual regions, they were not validated on complex cartilage morphology that typically occurs in osteoarthritis patients, they did not comprise follow-up evaluation nor evaluate the stability of the method by, for example, test–retest analysis. Importantly, none of these previous methods was designed for the separation of cartilage from synovial fluid, a crucial step to reduce intrasubject variability. In the newly developed method described herein, these main problems have been addressed. Indeed, the first challenge of using a stable registration reference was solved by employing bone surface as domains of the presence of cartilage. This was followed by a non-model-based segmentation, thus allowing delineation of complex and unpredictable cartilage morphology typical in pathological joints. Another important issue was the exclusion of the synovial fluid. This was possible using 3-D DESS MR images, which contain specific fluid information. In such images, the fluid is a very homogeneous and bright image area, which can be discriminated from the cartilage by using a Bayesian test. This contrasts with the use of other gradient echo MR sequences, e.g., 3-D-SPGR and 3-D-FISP, where it is virtually impossible to distinguish the synovial fluid from the cartilage by an automatic process; for these MR sequences only human expertise can be used to discriminate these two tissues.

A validation experiment with knee osteoarthritis patients and two visits (baseline and follow-up) demonstrated excellent correlations between semi-automatic and automatic segmented cartilage volume, not only for the global cartilage, but also for the femur and tibia. Correlation of cartilage volume and cartilage loss between the two visits also revealed excellent accuracy of automatic cartilage segmentation for global and femur pathological specimens. Test–retest validation also showed a very low error measurement level. These suggest that the developed automatic system is reliable and provides precise assessment of human osteoarthritic knee cartilage volume.

Cartilage degradation is the hallmark of osteoarthritis and its volume loss is related to the progression of the disease. The fully automatic method described herein provides accurate quantification of knee cartilage volume, and would, therefore, be useful not only for diagnosis, but also for clinical trials with patient follow-up.

Appendix I
Contrast and SGLD Matrix

This section details the contrast computation by the SGLD matricial technique. Let $\mathrm{I}(x, y)$ be an image, i and j be two gray levels and $v = [v_x, v_y]$ a vector. Computation of the SGLD matrix of I is noted as follows:

$$S(\mathrm{I}, v) = [S(\mathrm{I}, v)_{ij}] \tag{21}$$

where S is a matrix, whose indices correspond to gray levels i and j. The vector v is placed at all possible origins (x, y) in the image $\mathrm{I}(x, y)$ and we count how many times the following system (22) is true, and report it in the element $S(\mathrm{I}, v)_{ij}$

$$\begin{cases} \mathrm{I}(x, y) = i \\ \mathrm{I}(x + v_x, y + v_y) = j \end{cases}. \tag{22}$$

Hence, the element $S(\mathrm{I}, v)_{ij}$ tells how many times the origin voxel of v contains intensity i, while its destination voxel contains the intensity j. Relying on this resulting matrix storing the information about the texture of image $\mathrm{I}(x, y)$, we define specific operators to evaluate all the classical texture component characteristics such as homogeneity and contrast [36].

The contrast d of an SGLD matrix $S(\mathrm{I}, v)$ is defined by the following equation:

$$d(S(\mathrm{I}, v)) \equiv \sum_{i,j} |i - j|^2 S(\mathrm{I}, v)_{ij}. \tag{23}$$

To obtain a direction-independent contrast, the mean contrast over the four following vectors is computed; $v_1 = [1, 0]$, $v_2 = [0, 1]$, $v_3 = [1, 1]$, and $v_4 = [1, -1]$. The evaluation of the direction-independent contrast of SGLD matrix will be called contrast $\mathrm{cont}[\mathrm{I}]$ of I and given by

$$\mathrm{cont}[\mathrm{I}] \equiv \frac{1}{4} \sum_{k=1}^{k=4} d(S(\mathrm{I}, v_k)). \tag{24}$$

Appendix II
2-D Neighborhoods

To simplify the text, the layer of 3-D matrix J for a given height $h = f$ will be noted $J_f(u, v) \equiv J(u, v, h)/h = f$. It is a 2-D image defined by a 3-D image restriction.

Let B_t be a 1-D neighborhood of t of size α defined by

$$B_t \equiv \{s / |s - t| \leq \alpha\}. \tag{25}$$

Using this neighborhood, the 2-D neighborhood (B_u, B_v) centered on each point (u, v) exists, thus defining "stamps" $J_f(B_u, B_v)$ of $J_f(u, v)$ such that

$$J_f(B_u, B_v) \equiv \{J_f(u, v), u \in B_u, v \in B_v\}. \tag{26}$$

We can evaluate the contrast $C_f(u,v)$ of each individual stamp $J_f(B_u, B_v)$ of center (u,v) using the definition given in Appendix I of the contrast $\mathrm{cont}[J]$ of an image J

$$C_f(u,v) \equiv \mathrm{cont}[J_f(B_u, B_v)]. \tag{27}$$

The relation (27) is verified for all (x,y), thus the 2-D contrast matrix C_f has the same size as J_f. Basically, the size of the neighborhood was set to 5×5 voxels, $\alpha = 2$.

This definition can easily be transposed to 3-D images $J(u,v,h)$, as defined in (5). Analyzing the 2-D images obtained along each layer of distance h, we can express the local stamps $J(B_u, B_v, h)$ as follows:

$$J(B_u, B_v, h) \equiv \{J(u,v,h), u \in B_u, v \in B_v\} \tag{28}$$

thus compute the contrast matrix K of the entire image of normals J

$$K(u,v,h) = \mathrm{cont}[J(B_u, B_v, h)]. \tag{29}$$

Appendix III
Laplacian Edge Matrix

The Laplacian edge matrix of a 3-D image I is a binary matrix of discrete surfaces Δ, with $\Delta(i,j,k) = 1$ if (i,j,k) is on the interface. The matrix of surfaces is constructed by combining Laplacian images of contour evaluated on sagittal, coronal, and axial slices of image I. If $\Delta_{ij} = \partial^2/\partial i^2 + \partial^2/\partial j^2$ is the 2-D Laplacian operator, $*$ is the 2-D convolution operator, and G_{ij} is the Gaussian kernel, along the dimensions i and j, the set Δ is constructed as a sum of 2-D Laplacian operators of image I along each dimension

$$\begin{aligned} &\Delta(h,c,t) = 1 \\ &\text{if } \Delta_1(h,c,t) + \Delta_2(h,c,t) + \Delta_3(h,c,t) \geq 1 \text{ with} \\ &\quad \begin{cases} \Delta_1(h,c,t) = 1, \text{if } |\mathrm{I}_{z=t} * \Delta_{hc} G_{hc}| \leq \sigma \\ \Delta_2(h,c,t) = 1, \text{if } |\mathrm{I}_{x=h} * \Delta_{ct} G_{ct}| \leq \sigma \\ \Delta_3(h,c,t) = 1, \text{if } |\mathrm{I}_{y=c} * \Delta_{ht} G_{ht}| \leq \sigma. \end{cases} \end{aligned} \tag{30}$$

Appendix IV
Polyhedron Volume by Simplicial Decomposition

A simplex S_i is a tetrahedron generated by three noncollinear vectors $(\vec{a}, \vec{b}, \vec{c})$. If $\mathbf{P}(u,v,h)$ is a binary volume matrix associated with a polyhedron P, i.e., $P = \{(u,v,h)/\mathbf{P}(u,v,h) = 1\}$, a simplicial decomposition [37] of the polyhedron provides its decomposition into simplexes $S_i = \{(u,v,h)/\mathbf{S}_i(u,v,h) = 1\}$ such that

$$\mathbf{P}(u,v,h) = \sum_i S_i. \tag{31}$$

The volume of each simplex S_i is the volume of the simplex generated by $(\vec{a}, \vec{b}, \vec{c})$, given by

$$\mathrm{vol}(S_i) = \frac{1}{6} \det(\vec{a}, \vec{b}, \vec{c}) \tag{32}$$

where $\det$ is the determinant of the 3×3 matrix. Hence, the global volume of polyhedron P is given by

$$\mathrm{vol}(P) = \sum_i \mathrm{vol}(S_i). \tag{33}$$

Each of the height vertices of polyhedron P belongs to the set $\{\Phi^{\mathrm{mm}}(u \pm 1/2, v \pm 1/2, h \pm 1/2)\}$. Polyhedron P is constructed in our method as the reunion of two prisms, each prism decomposed in three tetrahedra [37].

Acknowledgment

The authors would like to thank the MRI technician of the Institut Universitaire de Gériatrie de Montréal, C. Hurst, for her valuable work on the MRI acquisition setup and procedure and to V. Wallis for her assistance with the manuscript preparation.

References

[1] J. Martel-Pelletier, D. Lajeunesse, and J. P. Pelletier, "Etiopathogenesis of osteoarthritis," in *Arthritis and Allied Conditions. A Textbook of Rheumatology*, 15th ed. W. J. Koopman and L. W. Moreland, Eds. Baltimore, MD: Lippincott, Williams and Wilkins, 2005, ch. 109, pp. 2199–2226.

[2] J. C. Buckland-Wright, "Quantitative radiography of osteoarthritis," *Ann. Rheum. Dis.*, vol. 53, pp. 268–275, 1994.

[3] M. Lequesne, T. Glimet, J. P. Massé, and J. Orvain, "Speed of the joint space narrowing (JSN) in primary medial osteoarthritis of the knee (OAK) over 3–5 years," *Osteoarthritis Cartilage*, vol. 1, pp. 23, 1993 (abstract).

[4] J. P. Raynauld, J. Martel-Pelletier, F. Abram, and J. P. Pelletier, "Use of quantitative magnetic resonance imaging in the cross-sectional and longitudinal evaluation of structural changes in knee osteoarthritis patients," in *Clinical Trials in Rheumatoid Arthritis and Osteoarthritis. Series: Clinical Trials*, D. M. Reid and C. G. Miller, Eds. London, U.K.: Springer-Verlag, 2008, pp. 235–248.

[5] J. P. Raynauld, J. Martel-Pelletier, M. J. Berthiaume, F. Labonté, G. Beaudoin, J. A. de Guise, D. A. Bloch, D. Choquette, B. Haraoui, R. D. Altman, M. Hochberg, J. M. Meyer, G. A. Cline, and J. P. Pelletier, "Quantitative magnetic resonance imaging evaluation of knee osteoarthritis progression over two years and correlation with clinical symptoms and radiologic changes," *Arthritis Rheum.*, vol. 50, pp. 476–487, 2004.

[6] F. Eckstein, C. Adam, H. Sittek, C. Becker, S. Milz, E. Schulte, M. Reiser, and R. Putz, "Non-invasive determination of cartilage thickness throughout joint surfaces using magnetic resonance imaging," *J. Biomech.*, vol. 30, pp. 285–289, 1997.

[7] F. Eckstein, M. Winzheimer, J. Hohe, K. H. Englmeier, and M. Reiser, "Interindividual variability and correlation among morphological parameters of knee joint cartilage plates: Analysis with three-dimensional MR imaging," *Osteoarthritis Cartilage*, vol. 9, pp. 101–111, 2001.

[8] A. Hyhlik-Dürr, S. Faber, R. Burgkart, T. Stammberger, K. P. Maag, K. H. Englmeier, M. Reiser, and F. Eckstein, "Precision of tibial cartilage morphometry with a coronal water-excitation MR sequence," *Eur. Radiol.*, vol. 10, pp. 297–303, 2000.

[9] C. G. Peterfy, C. F. van Dijke, D. L. Janzen, C. C. Glüer, R. Namba, S. Majumdar, P. Lang, and H. K. Genant, "Quantification of articular cartilage in the knee with pulsed saturation transfer subtraction and fat-suppressed MR imaging: Optimization and validation," *Radiology*, vol. 192, pp. 485–491, 1994.

[10] F. Cicuttini, A. Forbes, A. Asbeutah, K. Morris, and S. Stuckey, "Comparison and reproducibility of fast and conventional spoiled gradient-echo magnetic resonance sequences in the determination of knee cartilage volume," *J. Orthop. Res.*, vol. 18, pp. 580–584, 2000.

[11] L. R. Frank, E. C. Wong, W. M. Luh, J. M. Ahn, and D. Resnick, "Articular cartilage in the knee: Mapping of the physiologic parameters at MR imaging with a local gradient coil—Preliminary results," *Radiology*, vol. 210, pp. 241–246, 1999.

[12] R. Burgkart, C. Glaser, A. Hyhlik-Durr, K. H. Englmeier, M. Reiser, and F. Eckstein, "Magnetic resonance imaging-based assessment of cartilage loss in severe osteoarthritis: Accuracy, precision, and diagnostic value," *Arthritis Rheum*, vol. 44, pp. 2072–2077, 2001.

[13] A. E. Wluka, S. Stuckey, J. Snaddon, and F. M. Cicuttini, "The determinants of change in tibial cartilage volume in osteoarthritic knees," *Arthritis Rheum*, vol. 46, pp. 2065–2072, 2002.

[14] F. Eckstein, L. Heudorfer, S. C. Faber, R. Burgkart, K. H. Englmeier, and M. Reiser, "Long-term and resegmentation precision of quantitative cartilage MR imaging (qMRI)," *Osteoarthritis Cartilage*, vol. 10, pp. 922–927, 2002.

[15] F. Cicuttini, A. E. Wluka, A. Forbes, and R. Wolfe, "Comparison of tibial cartilage volume and radiologic grade of the tibiofemoral joint," *Arthritis Rheum*, vol. 48, pp. 682–688, 2003.

[16] S. Biswal, T. Hastie, T. P. Andriacchi, G. A. Bergman, M. F. Dillingham, and P. Lang, "Risk factors for progressive cartilage loss in the knee: A longitudinal magnetic resonance imaging study in forty-three patients," *Arthritis Rheum.*, vol. 46, pp. 2884–2892, 2002.

[17] J. P. Raynauld, C. Kauffmann, G. Beaudoin, M. J. Berthiaume, J. A. de Guise, D. A. Bloch, F. Camacho, B. Godbout, R. D. Altman, M. Hochberg, J. M. Meyer, G. Cline, J. P. Pelletier, and J. Martel-Pelletier, "Reliability of a quantification imaging system using magnetic resonance images to measure cartilage thickness and volume in human normal and osteoarthritic knees," *Osteoarthritis Cartilage*, vol. 11, pp. 351–360, 2003.

[18] J. Folkesson, E. Dam, O. Fogh Olsen, P. Pettersen, and C. Christiansen, "Automatic segmentation of the articular cartilage in knee MRI using a hierarchical multi-class classification scheme," in *Proc. MICCAI*, 2005, pp. 327–334.

[19] V. Grau, A. U. J. Mewes, M. Alcañiz, R. Kikinis, and S. K. Warfield, "Improved watershed transform for medical image segmentation using prior information," *IEEE Trans. Med. Imaging*, vol. 23, no. 4, pp. 447–457, Apr. 2004.

[20] J. Fripp, S. Crozier, S. K. Warfield, and S. Ourselin, "Automatic segmentation of articular cartilage in magnetic resonance images of the knee," *Int. Conf. Med. Image Comput. Assist. Interv.*, vol. 10, pp. 186–194, 2007.

[21] K. Li, S. Millington, X. Wu, and M. Sonka, "Simultaneous Segmentation of Multiple Closed Surfaces Using Optimal Graph Searching," *Proc. Int. Conf. Inf. Process. Med. Imaging*, vol. 3565, pp. 406–417, July, 2005.

[22] L. M. Lorigo, O. Faugeras, W. E. L. Grimson, R. Keriven, and R. Kikinis, "Segmentation of bone in clinical knee MRI using texture-based geodesic active contours," *Lect. Notes Comput. Sci.; Proc. First Int. Conf. MICCAI*, vol. 1496, pp. 1195–1204, 1998.

[23] R. Dalvi, R. Abugharbieh, D. C. Wilson, and D. Wilson, "Multi-contrast MR for enhanced bone imaging and segmentation," in *Proc. IEEE EMBS*, 2007, pp. 5620–5623.

[24] B. Godbout, C. Kauffmann, and J. A. de Guise, "Simple 2-D active contour model to segment non-convex objects in 3-D images," in *Proc. Vision Interface*, 1998, pp. 18–20.

[25] C. Lorenz and J. von Berg, "Fast automated object detection by recursive casting of search rays," *Int. Congr. Ser.*, vol. 1281, pp. 230–235, May 2005.

[26] G. P. Stachowiak, G. W. Stachiowiak, and P. Podsiadlo, "Automated classification of articular cartilage surfaces based on surface texture," in *Proc. Inst. Mech. Eng. [H]*, vol. 220, pp. 831–843, Nov. 2006.

[27] R. H. Hashemi, W. G. Bradley, and C. J. Lisanti, *MRI, The Basics*. Baltimore, MD: Lippincott Williams and Wilkins, 2003.

[28] F. Eckstein, F. Cicuttini, J. P. Raynauld, J. C. Waterton, and C. Peterfy, "Magnetic resonance imaging (MRI) of articular cartilage in knee osteoarthritis (OA): Morphological assessment," *Osteoarthritis Cartilage*, vol. 14, pp. A46–A75, 2006.

[29] F. Eckstein, M. Hudelmaier, W. Wirth, B. Kiefer, R. Jackson, J. Yu, C. Eaton, and E. Schneider, "Double echo steady state (DESS) magnetic resonance imaging of knee articular cartilage at 3 Tesla: A pilot study for the Osteoarthritis Initiative," *Ann. Rheum. Dis.*, vol. 65, pp. 433–441, 2006.

[30] P. A. Hardy, M. P. Recht, D. Piraino, and D. J. Thomasson, "Optimization of a dual echo in the steady state (DESS) free-precession sequence for imaging cartilage," *Magn. Reson. Imaging*, vol. 6, pp. 329–335, 1996.

[31] C. Kauffmann, P. Gravel, B. Godbout, A. Gravel, G. Beaudoin, J. P. Raynauld, J. Martel-Pelletier, J. P. Pelletier, and J. A. de Guise, "Computer-aided method for quantification of cartilage thickness and volume changes using MRI: Validation study using a synthetic model," *IEEE Trans. Biomed. Eng.*, vol. 50, no. 9, pp. 978–988, Aug. 2003.

[32] N. Otsu, "A threshold selection method from gray-level histograms," *IEEE Trans. Syst., Man, Cybern.*, vol. 9, no. 1, pp. 62–66, Jan. 1979.

[33] Z. Zhang, "Iterative point matching for registration of free-form curves and surface," *Int. J. Comput. Vis.*, vol. 13, pp. 119–152, 1994.

[34] R. Altman, E. Asch, D. Bloch, G. Bole, D. Borenstein, K. Brandt, W. Christy, T. D. Cooke, R. Greenwald, M. Hochberg, D. Howell, D. Kaplan, W. Koopman, S. Longley III, H. Mankin, D. J. McShane, T. Medsger Jr., R. Meenan MD, W. Mikkelsen, R. Moskowitz, W. Murphy, B. Rothschild, M. Segal, L. Sokoloff, and F. Wolfe, "Development of criteria for the classification and reporting of osteoarthritis. Classification of osteoarthritis of the knee," *Arthritis Rheum*, vol. 29, pp. 1039–1049, 1986.

[35] J. Eng, "Sample size estimation: How many individuals should be studied?," *Radiology*, vol. 227, pp. 309–313, May 2003.

[36] A. A. Qazi, J. Folkesson, P. C. Pettersen, M. A. Karsdal, C. Christiansen, and E. B. Dam, "Separation of healthy and early osteoarthritis by automatic quantification of cartilage homogeneity," *Osteoarthritis Cartilage*, vol. 15, pp. 1199–1206, 2007.

[37] K. Erleben, H. Dohlmann, and J. Sporring, "The adaptive thin shell tetrahedral mesh," *J. WSCG*, vol. 13, pp. 17–24, 2005.

Authors' photographs and biographies not available at the time of publication.